



Martensitic transformation, magnetic entropy, and adiabatic temperature changes in bulk and ribbon $\text{Ni}_{48}\text{Mn}_{39.5}\text{Sn}_{12.5-x}\text{In}_x$ ($x = 2, 4, 6$) metamagnetic shape memory alloys

P. Czaja^{1,a)} , J. Przewoźnik², L. Hawelek³, A. Chrobak⁴, P. Zackiewicz³, W. Maziarz¹

¹The Aleksander Krupkowski Institute of Metallurgy and Materials Science, Polish Academy of Sciences, 25 Reymonta St, 30-059 Kraków, Poland

²Department of Solid State Physics, Faculty of Physics and Applied Computer Science, AGH University of Science and Technology, Al. Mickiewicza 30, 30-059 Kraków, Poland

³Łukasiewicz Research Network - Institute of Non-Ferrous Metals, 5 Sowinskiego Str, 44-100 Gliwice, Poland

⁴The A. Chelkowski Institute of Physics, University of Silesia, 4 Uniwersytecka Str, 40-007 Katowice, Poland

^{a)}Address all correspondence to this author. e-mail: p.czaja@imim.pl

Received: 19 May 2021; accepted: 5 August 2021; published online: 30 August 2021

Martensitic transformation, magnetic entropy, and direct adiabatic temperature changes in $\text{Ni}_{48}\text{Mn}_{39.5}\text{Sn}_{12.5-x}\text{In}_x$ ($x = 2, 4, 6$) metamagnetic Heusler bulk and grain-constrained ribbon alloys were studied. All alloys showed a typical $L2_1$ structure in austenite and the 4O structure in martensite. Their relative volume contributions changed depending on In content. With increasing In concentration, the martensitic transformation temperature increased, whereas the Curie temperature of austenite decreased. The magnetic entropy change under magnetic field of 5 T attained maximum of 20 J/kgK in the bulk and 14.4 J/kgK in the ribbon alloys with the $\text{Ni}_{48}\text{Mn}_{39.5}\text{Sn}_{8.5}\text{In}_4$ nominal composition. The corresponding adiabatic temperature change under 1.7 T yielded 1.3 K for the $\text{Ni}_{48}\text{Mn}_{39.5}\text{Sn}_{8.5}\text{In}_4$ bulk alloy. Despite grain confinement, melt spinning was found to stabilize martensite phase. Changes observed were discussed with relation to strengthened covalency imposed by In substitution.

Introduction

Ni–Mn–Sn–(In, Sb) metamagnetic Heusler alloys have recently aroused interest as prospective materials for environmentally friendly magnetic refrigeration. This is due to an inverse magnetocaloric effect occasioned in this instance by the change in magnetization (ΔM), which takes place during the first-order martensitic phase transformation (MT) [1]. Both the MT temperature (T_{MT}) and the ΔM have been found sensitive to either (i) the valence electron to atom ratio (e/a) or (ii) the chemical pressure effect expressed in terms of an austenite unit cell volume (V_c). The latter has the capacity to override the influence of e/a [2, 3]. In general, such a susceptibility has electronic origins [4], and it derives from the magnetic contribution to the Gibbs free energy change that stabilizes the more ferromagnetic phase [5]. Typically in the Ni–Mn–Sn and in the Ni–Mn–In systems, the T_{MT} increases with increasing e/a and decreasing unit cell volume; thus for both systems, the functional behavior can be easily optimized by altering the stoichiometry or by introduction

of a substituting element [6–8]. A number of different elements replacing for instance Sn in the Ni–Mn–Sn and including Al [9, 10], Ga [11], Ge [12–15], and Sb [16] have been studied.

Typically, the Ni–Mn–Sn–(In) alloys appear to conform to the e/a and the chemical pressure rules, with some exception for Mn-rich alloys [17]. For such alloys with excess Mn content, the main driving force for the T_{MT} change is associated with hybridization between the Ni 3d and the 3d states of surplus Mn located at Sn sites. Hence, any change in Ni or Mn content, either by substitution or stoichiometry change, can effectively weaken hybridization and reduce T_{MT} [17, 18]. Interestingly, the T_{MT} and the Curie temperature of the martensite phase (T_{C}^{M}) in the $\text{Ni}_{50}\text{Mn}_{50-x}\text{In}_x$ alloys were reported to decrease more drastically with increasing In content than with Sn or Sb in the corresponding $\text{Ni}_{50}\text{Mn}_{50-x}\text{Sn}_x$ and $\text{Ni}_{50}\text{Mn}_{50-x}\text{Sb}_x$ systems. Simultaneously theoretical first principle calculations predicted an increase of the T_{MT} in the $\text{Ni}_8\text{Mn}_6\text{Sn}_{2-x}\text{In}_x$ alloy when Sn is replaced with In. It was attributed to hybridization of the Ni 3d and In 5p

states, which leads to a decrease in the density of states near the Fermi level [19]. As it happens, it is in apparent contradiction to the established e/a and the unit cell volume rules, since In has less valence electrons and larger atomic radius than Sn [20]. Nonetheless, in consistence with theoretical predictions, more experimental studies on, *e.g.*, the quinary $\text{Ni}_{45}\text{Co}_5\text{Mn}_{40}\text{In}_x\text{Sn}_{10-x}$ alloy confirmed an increase of the T_{MT} and a decrease of the Curie temperature of austenite (T_{C}^{A}) with increasing In content [21]. Simultaneously partial substitution (8 at.%) of In by Sn in the $\text{Ni}_{50}\text{Mn}_{34}\text{Sn}_{18}$ alloy led to a decrease in the unit cell volume while elevating the T_{MT} and the T_{C}^{A} temperatures in agreement with the chemical pressure effect [22]. Therefore, in view of the many contradictory results and in order to bring more consistency to experimental evidence and hence shed more light the physical basis behind the e/a and v_{c} influences, we have systematically examined the evolution of structure, characteristic transformation temperatures, and magnetic and magnetocaloric properties of the $\text{Ni}_{48}\text{Mn}_{39.5}\text{Sn}_{12.5-x}\text{In}_x$ ($x = 2, 4, 6$) alloys. The magnetic entropy changes ($\Delta S_{\text{transf.}}^{\text{mag}}$) have been calculated and set against the measured adiabatic temperature change (ΔT_{ad}) to evaluate the real cooling power of the studied alloys. The scrutinized alloys have been produced by conventional metallurgy and by melt spinning technique to ensure lack of interference from chemical inhomogeneity and to compare the magnetocaloric response of bulk and grain-constrained ribbon materials. In addition, ribbons due to their intrinsic brittleness become attractive for 3D printing technology as a viable powder source; hence, more studies assessing their functional performance are welcomed.

Results

The X-ray diffraction patterns for the $\text{Ni}_{48}\text{Mn}_{39.5}\text{Sn}_{12.5-x}\text{In}_x$ ($x = 2, 4, 6$) bulk and ribbon alloys collected at room temperature are presented in Fig. 1a and b. It was found that except for the In6 ribbon, all the samples contain a mixture of the $L2_1$ austenite ($Fm\bar{3}m$) and the 4O martensite ($Pmma$) structures. The unit cell volume and relative mass contribution of each of the two phases clearly vary with composition (Fig. 1c, d). Table 1 collects lattice parameters, unit cell volumes (V_{c}), and relative mass contributions of austenite phase (p_{c}) for all alloys. For illustration the latter, two parameters were also presented as a function of In content in Fig. 1c and d. The figures also show reference results for ternary In0 alloy, published elsewhere [10]. In general, for the bulk alloys, the V_{c} is found stable up to 4 at.% In, and then it falls considerably. For the ribbon alloys with 2 at.% In substitution, V_{c} first decreases and then increases, when the content of In goes up to 4 at.%. The increase in the unit cell volume is consistent with the fact that the atomic radius of In (155 pm) is larger than the atomic radius of Sn (145 pm). In parallel with the unit cell volume change, the p_{c} progressively decreases with

increasing In for Sn substitution except for the bulk In2 and In4 alloys. Furthermore, it may be observed that p_{c} is significantly reduced, by about 62% and 64% for both bulk and ribbon alloys already upon 2 at.% In for Sn substitution when compared to the In0 sample. It is also seen that the 100% martensitic transformation is reached at room temperature with the In6 ribbon sample. In order to complement the XRD analysis, the example selected area electron diffraction patterns (SADP) for the most interesting In4 bulk and ribbon samples are shown in Fig. 1e–g. In the bulk alloy, the $L2_1$ austenite phase, indexed along the [010] zone axis, was found to coexist with the martensite phase of 4O structure, identified along the [012] zone axis, whereas the In4 ribbon appeared predominantly martensitic with the 4O structure indexed along the [010] direction. Fig. 1h shows a bright-field (BF) image with a typical microstructure for Heusler Ni–Mn base ribbons having grain with average size of $\sim 1.5 \mu\text{m}$ [10, 23].

The DSC curves for all the bulk and ribbon samples recorded under cooling and heating cycles are presented in Fig. 2a and b. In consistence with structural analysis, all the samples undergo a reversible MT, which is well manifested by exo- and endothermic peaks on cooling and on heating, respectively. The characteristic martensitic transformation temperatures including martensite start (M_{s}), finish (M_{f}) and austenite start (A_{s}), finish (A_{f}) along with the transformation hysteresis ($A_{\text{f}} - M_{\text{s}}$) and the peak temperature of the forward austenite \rightarrow martensite transformation ($T_{\text{p}}^{\text{A}\leftrightarrow\text{M}}$) were determined by the tangent method and from the peak's maximum on the DSC curves. They are collected in Table 2. The table also contains the Curie temperature of austenite (T_{C}^{A}) and martensite (T_{C}^{M}) obtained from the inflection points on the thermo-magnetization measurements—discussed later—and the fitted Curie–Weiss temperatures for austenite ($\theta_{\text{C}}^{\text{A}}$) and martensite ($\theta_{\text{C}}^{\text{M}}$). Both the T_{C}^{A} and T_{C}^{M} are in good agreement with the respective Curie–Weiss $\theta_{\text{C}}^{\text{A}}$ and $\theta_{\text{C}}^{\text{M}}$ temperatures. The magnitudes of the transformation entropy changes ($\Delta S_{\text{transf.}}^{\text{A}\leftrightarrow\text{M}}$), evaluated as the ratio of the measured enthalpy change ($\Delta H_{\text{transf.}}^{\text{A}\leftrightarrow\text{M}}$) and the peak temperature for the forward and reverse transformation ($T_{\text{transf.}}^{\text{A}\leftrightarrow\text{M}}$), *i.e.*, $\Delta S_{\text{transf.}}^{\text{A}\leftrightarrow\text{M}} = \Delta H_{\text{transf.}}^{\text{A}\leftrightarrow\text{M}} / T_{\text{transf.}}^{\text{A}\leftrightarrow\text{M}}$, were collected too and are given in Fig. 2c as a function of In content. Overall it was found that the $T_{\text{p}}^{\text{A}\leftrightarrow\text{M}}$ temperatures in all the samples increase with the increase of In for Sn substitution. It was also found that the $T_{\text{p}}^{\text{A}\leftrightarrow\text{M}}$ temperatures are higher for ribbon than for bulk alloys (Fig. 2d) with the equivalent nominal composition, what is in contrast to typical observations [10, 23]. Additionally, the jerky like appearance of the DSC peak detected upon heating for the In4 bulk sample may be associated with local compositional inhomogeneity or multiple martensitic transformations, which could also justify peak spread and tailing effects [24]. In view of thermal stability concerns under prolonged aging treatment [25, 26], the bulk alloys were annealed at 1170 K and at 1070 K for the same length of time (24 h). Regardless of temperature applied, the $\Delta S_{\text{transf.}}^{\text{A}\leftrightarrow\text{M}}$ remains

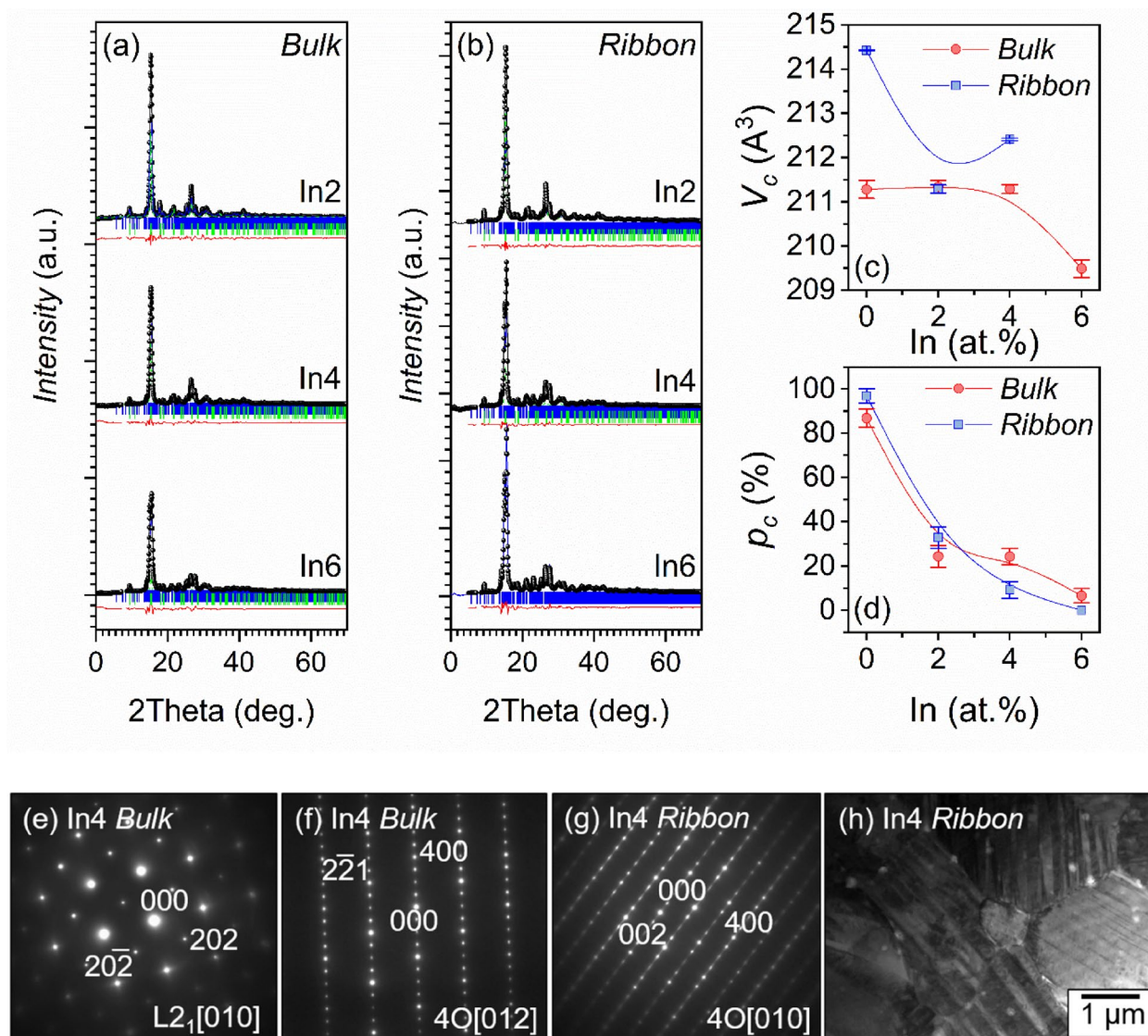


Figure 1: X-ray diffraction patterns collected at room temperature for $\text{Ni}_{48}\text{Mn}_{39.5}\text{Sn}_{12.5-x}\text{In}_x$ ($x = 2, 4, 6$) bulk (a) and ribbon (b) alloys. The unit cell volume of austenite V_c (c) and the relative volume fraction of austenite p_c (d) as a function of In concentration. The selected area electron diffraction patterns taken from the In4 bulk (e), (f), and In4 ribbon (g) samples. The bright-field image taken from the In4 ribbon sample (h).

comparable for the In2 and In4 alloys, but it differs quite considerably between the two temperatures for the In6 alloy (Fig. 2c). Since no other phase was detected by XRD, the eutectoid type phase decomposition was then excluded and the results could be understood in relation to the different degrees of ordering of the alloy, which alter magnetization output. The magnetic contribution to the structural transformation entropy change $\Delta S_{\text{transf}}^{A \leftrightarrow M}$, given the opposite signs of magnetic and structural contribution, justifies the difference in the values of the total transformation entropy change between the forward and reverse transformations, the difference gets larger when $A_s \ll T_C^A$ [27].

Figure 3a and b shows temperature-dependent magnetization measured under 5 T magnetic field for bulk and ribbon

$\text{Ni}_{48}\text{Mn}_{39.5}\text{Sn}_{12.5-x}\text{In}_x$ ($x = 2, 4, 6$) alloys in zero field cooled (ZFC) and field cooled (FC) modes. The ZFC entailed cooling sample down to 4 K under no magnetic field and then switching on the field and measuring the magnetization on heating up to 350 K with the field fixed. The FC curve was subsequently obtained by measuring the magnetization on cooling the sample again down to 4 K with the field set constant. The magnetic susceptibility and magnetization evolve in a typical fashion for metamagnetic shape memory alloys [28]. Following the FC protocol from the high-temperature paramagnetic range, the magnetization first increases, when the temperature coincides with the T_C^A , and then as the temperature goes down the magnetization drops around the $T_p^{A \leftrightarrow M}$. The increase in magnetization at

TABLE 1: Lattice parameters of austenite (a_o , b_o , c_o) and unit cell volume of austenite (V_o) and martensite (V_o), relative mass contribution of the austenite phase (p_c) in $Ni_{48}Mn_{39.5}Sn_{12.5-x}In_x$ ($x=0, 2, 4, 6$) bulk and ribbon alloys.

Alloy	Austenite			Martensite			
	a_c (Å)	V_c (Å ³)	p_c (%)	a_o (Å)	b_o (Å)	c_o (Å)	V_o (Å ³)
In0*							
Bulk	5.9560(4)	211.28(2)	86.8(4.3)	8.585(15)	5.656(10)	4.320(10)	209.7(7)
Ribbon	5.9854(1)	–	96.9(3.2)	8.620(5)	5.656(4)	4.360(5)	–
In2							
Bulk	5.9565(22)	211.34(0.14)	24.4(4.9)	8.5159(55)	5.6504(50)	4.3363(33)	208.66(28)
Ribbon	5.9561(15)	211.29(0.09)	32.8(4.8)	8.5635(35)	5.6459(30)	4.3403(23)	209.85(18)
In4							
Bulk	5.9561(16)	211.29(0.10)	24.3(3.7)	8.5601(38)	5.6446(33)	4.3460(24)	209.99(0.19)
Ribbon	5.9666(47)	212.41(0.29)	9.2(3.7)	8.5778(35)	5.6287(22)	4.3459(23)	209.83(0.16)
In6							
Bulk	5.9391(58)	209.49(0.35)	6.6(3.2)	8.5641(39)	5.6147(32)	4.3537(25)	209.34(0.20)
Ribbon	–	–	–	8.5810(25)	5.6024(17)	4.3629(19)	209.74(0.13)

* Ref. [10].

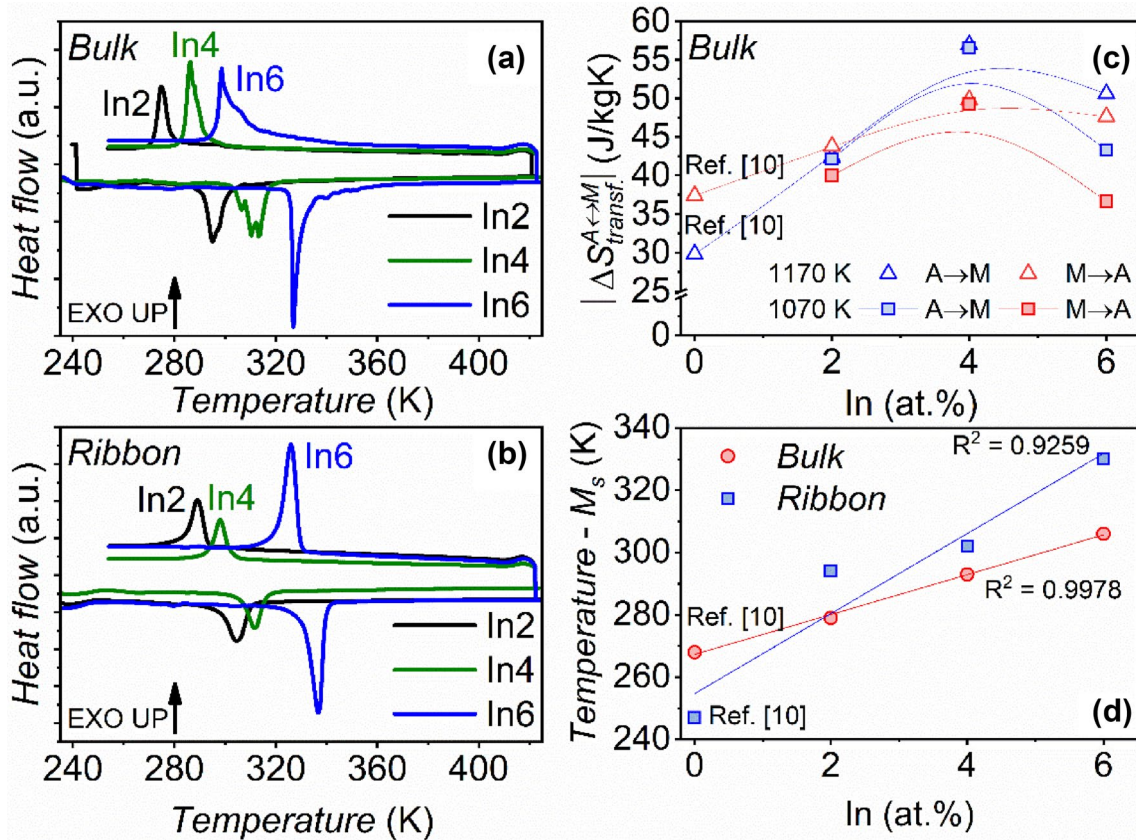


Figure 2: DSC curves upon cooling and heating cycles as a function of temperature for bulk annealed at 1070 K (a) and as melt-spun In2, In4, and In6 ribbons (b). EXO UP↑. The absolute value of the forward and reverse martensitic transformation entropy changes— $|\Delta S_{transf}^{A \leftrightarrow M}|$ as a function of In content (c) and the martensite start transformation temperature— M_s as a function of In content (d) for the studied In2, In4, and In6 bulk and ribbon alloys.

low temperature, below M_p , announces the pending approach to T_C^M . The splitting between the ZFC and FC curves below T_C^M is explained by the coexisting antiferromagnetic and ferromagnetic states in the low-temperature martensite phase [14, 28]. On heating (ZFC), the behavior is reversed with typical

hysteresis around the $T_p^{A \leftrightarrow M}$. All the examined alloys conform well to this general behavior, yet they differ in terms of the magnitude of magnetization response in both austenite and martensite states. From Fig. 3a, one may see that in the bulk

TABLE 2: The characteristic martensite start (M_s), martensite finish (M_f), austenite start (A_s), austenite finish (A_f) transformation temperatures, the transformation hysteresis ($A_f - M_s$), the Curie temperature of austenite (T_C^A) and martensite (T_C^M), the fitted Curie–Weiss temperature for aus-

tenite (θ_C^A) and martensite (θ_C^M), and the peak temperature of the forward austenite \rightarrow martensite transformation ($T_p^{A \rightarrow M}$) for bulk alloys annealed at 1070 K and as melt-spun ribbons.

Alloy	M_s (K)	M_f (K)	A_s (K)	A_f (K)	$A_f - M_s$ (K)	T_C^A (K)	θ_C^A (K)	$T_p^{A \rightarrow M}$ (K)	T_C^M (K)	θ_C^M (K)
In2										
Bulk	279	271	290	302	23	300	302	275	201	195
Ribbon	294	284	298	311	17	302	310	290	209	206
In4										
Bulk	293	283	303	318	25	298	302	287	185	187
Ribbon	302	293	306	316	14	301	301	299	188	193
In6										
Bulk	306	296	326	332	26	291	280	302	162	–
Ribbon	330	320	330	340	10	–	305	326	148	179

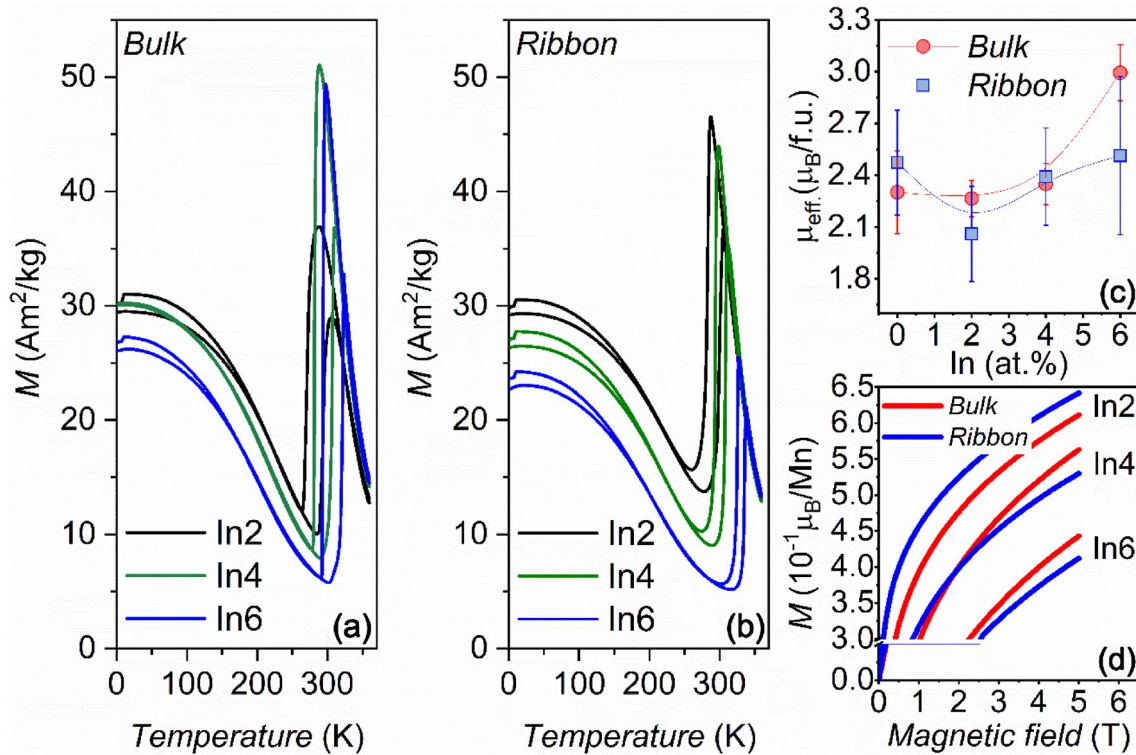


Figure 3: Temperature-dependent ZFC, FC magnetization measured under the applied magnetic field of 5 T for $Ni_{48}Mn_{39.5}Sn_{12.5-x}In_x$ ($x = 2, 4, 6$) for the bulk (a) and ribbon (b) alloys. The effective magnetic moment (c) and magnetization at 4 K (d) for the bulk and ribbons In2, In4, and In6 alloys.

alloys, the magnetization in the austenite state is the highest in the In4 alloy and then it gets lower with the In6 and In2 alloys, whereas in the martensite state, the magnetization decreases systematically from the In2 down to the In6 alloy. On the other hand, in ribbon alloys, the magnetization decreases in both martensite and austenite phase proportionally to the increasing In content. The effective magnetic moment of the compound magnetic atom of austenite (μ_{eff}^A), determined from the inverse of the paramagnetic susceptibility vs. temperature measurements

at 5 mT—not shown, for ribbon and bulk alloys is plotted as a function of In concentration in Fig. 3c. The μ_{eff}^A shows moderate variation with changing In concentration up to 4 at.% in bulk alloys, while it varies slightly more in ribbons up to 6 at.% of In. Large change in μ_{eff}^A is noted in the case of the In6 bulk sample. On the whole, the value of μ_{eff}^A corresponds to typical values reported for Ni–Mn base metamagnetic shape memory alloys [14]. In order to assess the magnetization response of martensite phase, the isothermal magnetization, per Mn atom, curves at 4 K

with the field in the range up to 5 T were collected in Fig. 3d. From the figure, it becomes evident that magnetization does not saturate even at 5 T and it decreases with increasing In concentration being on the whole larger, with the exception for In2, in the bulk than in the ribbon alloys. Overall from the thermomagnetization measurements, it was found that on heating the weakly magnetic martensite transitions into initially ferromagnetic (FM) austenite, which goes paramagnetic at higher In content ($T_{MT} > T_C^A$).

The typical metamagnetic transition from weakly magnetic martensite to austenite is well resolved on the isothermal magnetization curves (Fig. 4) recorded for all the studied alloys at temperatures close to their respective $T_p^{A \leftrightarrow M}$. The largest magnetization values and magnetic hysteresis loops were found for the In4 bulk sample and then for the In2 alloy. Among the ribbons, the In2 and In4 alloys demonstrated comparable response in terms of maximum magnetization attained under 5 T, whereas the largest loops were recorded with the In4 ribbons. On the contrary, the In6 alloy showed the weakest susceptibility of the reverse martensitic transformation to the magnetic field applied, what indicated a small magnetization difference (ΔM) between austenite and martensite in this alloy. Based on the isothermal magnetization measurements, the magnetic entropy

changes ($\Delta S_{transf.}^{mag.}$) were evaluated through the Maxwell relation: $\Delta S_{transf.}^{mag.} = \mu_0 \int_0^H \left(\frac{\partial M}{\partial T} \right)_H dH$, where M is magnetization, H is the magnetic field applied, and T is temperature. The results for bulk and ribbon alloys under magnetic field of 5 T are presented in Fig. 5a and b. The insets in both figures show dependence of the $\Delta S_{transf.}^{mag.}$ on the magnetic field. The magnetic entropy increased with increasing magnetic field (insets in Fig. 5a and b). The largest magnetic entropy change is noted for the bulk In4 sample ~ 20.4 J/kgK, while for the bulk In2 and In6 samples, it assumed ~ 11 J/kgK and 11.6 J/kgK, respectively. For the ribbon samples, the $\Delta S_{transf.}^{mag.}$ correspondingly peaked at 14.4 J/kgK for the In4 and at 10.8 J/kgK for the In2 and at 3.5 J/kgK for the In6 samples. The results of the adiabatic temperature changes are shown in Fig. 5c–e. As expected, the largest ΔT_{ad} among the studied alloys is measured for the In4 alloy ~ 1.3 K, whereas the In2 gives 1.0 K and the In6 yields the lowest temperature change of 0.6 K. The ΔT_{ad} increases with increasing magnetic field and for better visibility and comparison with the ΔT_{ad} , the $\Delta S_{transf.}^{mag.}$ as a function of In content under applied magnetic fields of 1.7 T and 5 T are plotted together in Fig. 5f. Interestingly the $\Delta S_{transf.}^{mag.}$ under 1.7 and 5 T was at the similar level in the In2 bulk and ribbon and in the In6 ribbon alloys under 1.7 T. The disparity was more pronounced for the In4

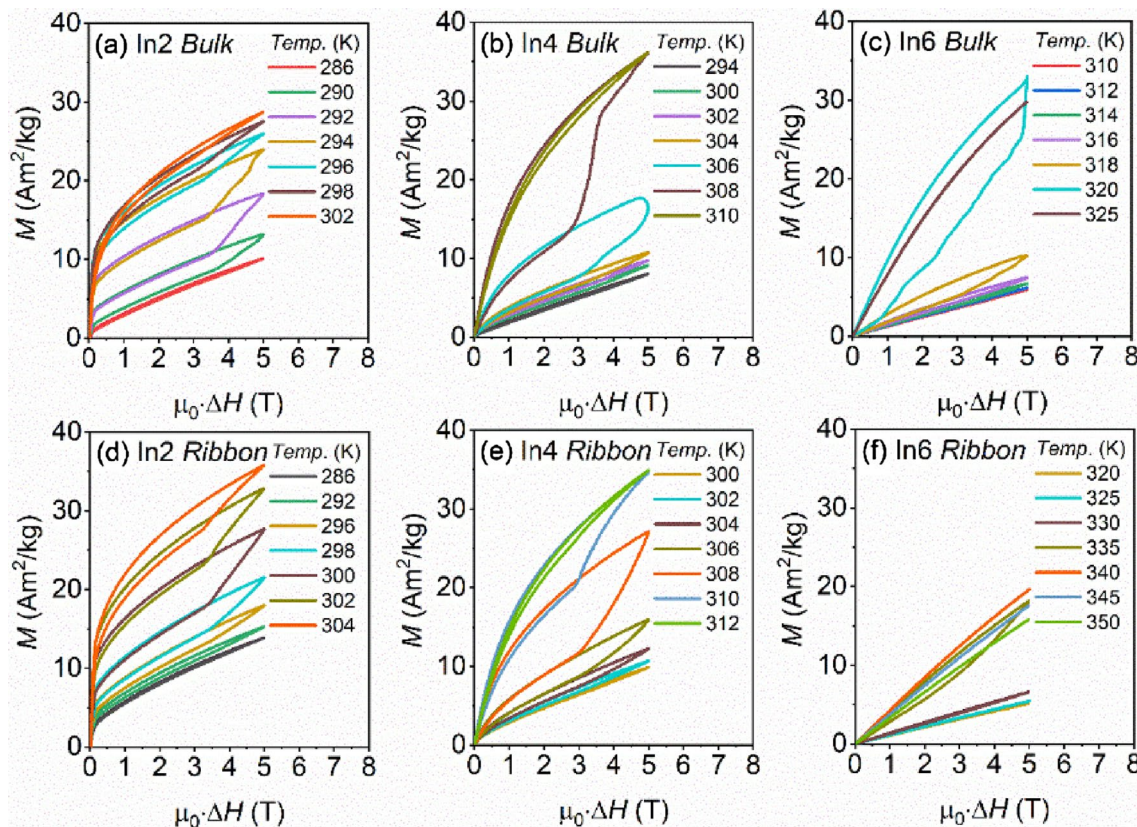


Figure 4: Magnetization isotherms $M(H)$ measured under the applied magnetic field change of 0–5 T at temperatures around T_M for $Ni_{48}Mn_{39.5}Sn_{12.5-x}In_x$ ($x=2, 4, 6$) bulk and ribbon alloys.

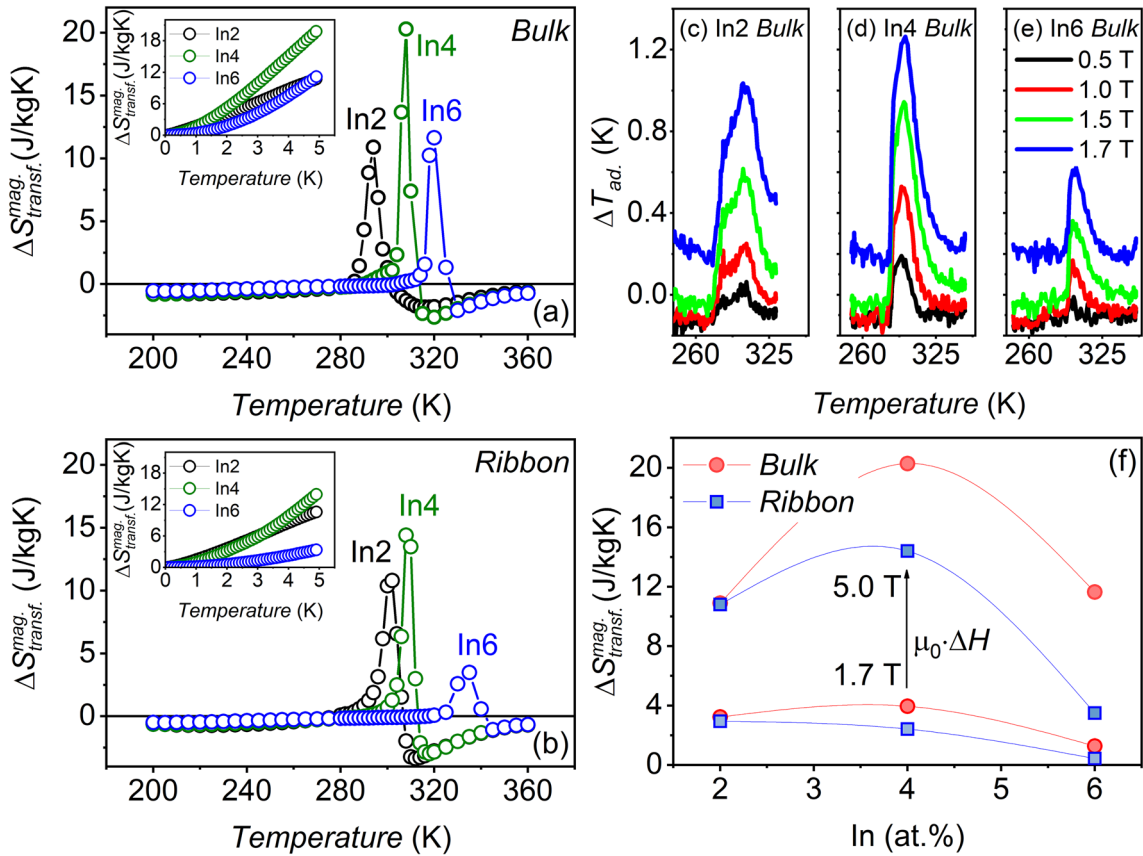


Figure 5: Magnetic entropy change ΔS_M as a function of temperature under different magnetic fields of 1 to 5 T for $\text{Ni}_{48}\text{Mn}_{39.5}\text{Sn}_{12.5-x}\text{In}_x$ ($x=2, 4, 6$) bulk (a) and ribbon (b) alloys. The adiabatic temperature change ΔT_{ad} , as a function of temperature for the In2 (c), In4 (d), and In6 (e) bulk samples under magnetic field change within the range of 0.5–1.7 T. The magnetic entropy change $\Delta S_{transf}^{A \leftrightarrow M}$ as a function of In content under magnetic fields of 1.7 T and 5 T for the studied $\text{Ni}_{48}\text{Mn}_{39.5}\text{Sn}_{12.5-x}\text{In}_x$ bulk and ribbon samples.

alloy, and it extended with the applied magnetic field. Assuming circa a fivefold ΔS_{transf}^{mag} increase with increasing magnetic field from 1.7 T to 5 T and a linear scaling between the ΔS_{transf}^{mag} and ΔT_{ad} , circa 6.5 K temperature change would be then effectively expected under 5 T, what might be attractive for solid-state refrigeration.

Discussion

It is well established that the unique properties of the Heusler-based off-stoichiometric Ni–Mn–Sn alloys are closely related to the strong coupling between magnetic and structural degrees of freedom and they are attached to the thermo-elastic MT [1, 29–31]. The magnetization difference between austenite and martensite taking part in MT is the driving force for magnetic field-induced reverse MT. It is given by the Zeeman energy $E = \mu_0 \Delta M \cdot H$ [32–35]. Since, the magnetic moment in such alloys is mainly attributed to the Mn atoms, coupled via the oscillatory Ruderman–Kittel–Kasuya–Yosida (RKKY) interactions [36], the magnetic properties and magnetic ordering temperatures are sensitive to the $d_{Mn} - d_{Mn}$ distance [37, 38].

It is widely acknowledged for many Heusler systems that for a particular alloy composition, the T_{MT} is related to its electronic structure. For experimental convenience, it is often expressed in terms of the valence electron concentration per atom e/a ; taken in fact as the concentration weighted sum of the s , p , and d electrons [2]. In general, T_{MT} exhibits a linear dependence on e/a and for a number of Ni–Mn–Sn base alloys, the T_{MT} is found to increase, whereas the T_C^A decreases with increasing e/a [6, 33, 39–41]. While on decreasing e/a , such as in the case of Co for Ni substitution [8, 42–44], T_{MT} was found to decrease. The increase of T_C^A in this instance was ascribed to the stronger Co–Mn than Ni–Mn exchange interactions. An overview of the mutual dependence of T_{MT} , T_C^A and e/a for a range of quaternary alloys is shown in Table 3. From the table, it is seen that that both the characteristic transition temperatures not always conform to the e/a rule.

Interestingly, a non-monotonic dependence of T_{MT} on e/a was reported in $\text{Ni}_{50}\text{Mn}_{30-x}\text{Cu}_x\text{Sn}_{15}$ system, where Cu substitution in the amount of 2 and 5 at.% yielded initially a slight increase in T_C^A with a profound drop in T_{MT} . Further increase in Cu content up to 10 at.% yielded a decrease

TABLE 3: An overview of the effect of changing composition on the T_{MT} , T_C^A and e/a for a range of quaternary alloys.

Alloy	T_{MT}	T_C^A	e/a	Ref
$Ni_{50-x}Cu_xMn_{36}Sn_{14}$	↓	↑	↑	[45]
$Ni_{50-x}Cu_xMn_{38}Sn_{12}$	↓	↑	↑	[46]
$Ni_{46-x}Cu_xMn_{43}Sn_{11}$	↓	↑	↑	[47]
$Ni_{43}Mn_{46-x}Co_xSn_{11}$	↓	↑	↑	[48]
$Ni_{50}(Mn_{1-x}Fe_x)_{36}Sn_{14}$	↓	↑	↑	[38]
$Ni_{45}Mn_{44-x}Cr_xSn_{11}$	↓	–	↓	[49, 50]
$Mn_{48-x}Ti_xNi_{42}Sn_{10}$	↓	↓	↓	[51]
$Ni_{43}Mn_{46-x}V_xSn_{11}$	↓	Marginal	↓	[52]
$Ni_{43}Mn_{46}Sn_{11}B$	↑	↑	–	[53]

Arrow indicates either an increase (↑) or a decrease (↓) in the relevant parameter.

in T_C^A and resulted in suppression of the MT [54]. On the other hand, replacement of Mn by little amount of Cu $\leq 3\%$ in $Ni_{43}Mn_{46-x}Cu_xSn_{11}$ resulted in considerable shift of T_{MT} upwards [55]. Along the electronic structure modifications also, structural geometry change is noted as a factor affecting both T_{MT} and T_C^A temperatures. For instance, the isoelectronic substitution by an element with the same number of valence electrons but lower atomic radii may result in unit cell volume reduction, which can increase T_{MT} and simultaneously decrease T_C^A as was shown for $Ni_{43}Mn_{46}Sn_{11-x}Ge_x$ [12], $Mn_2Ni_{1.6}Sn_{0.4-x}Ge_x$ [13], and $Ni_{43}Mn_{46}Sn_{11-x}Si_x$ [56] alloys. This effect may arise from the modified $d_{Mn}-d_{Mn}$ distance and stronger hybridization between Ni and Mn atoms in a reduced unit cell volume leading to higher density of states (DOS) near the Fermi level, which may then promote MT. Accordingly, increase of lattice parameter such as in Pd for Ni substituted $Ni_{50-x}Pd_xMn_{37}Sn_{13}$ was reported to result in a simultaneous decrease of T_{MT} and T_C^A , potentially due to a decrease in the Ni–Mn exchange interaction originating in increased lattice constant [57]. Furthermore, it was shown that the chemical pressure effect may even in some cases compete and dominate the e/a such as in Al substituted $Ni_{43}Mn_{46}Sn_{11-x}Al_x$ [9], $Ni_{48}Mn_{39.5}Sn_{12.5-x}Al_x$ [10, 58], and $Ni_2Mn_{1.36}Sn_{0.64-x}Al_x$ [59] alloys, where despite decreasing e/a , the T_{MT} increased and T_C^A remained almost unchanged. Predominantly due to contraction of the unit cell given smaller than Sn atomic radius of Al, this agreed with theoretical calculations [60]. It was also shown that in $Ni_2Mn_{1+x}Sn_{1-x}$ system T_C^A increases with increasing pressure [61], whereas in $Ni_{50-x}Mn_{37+x}Sn_{13}$ [62] alloys, the application of external pressure shifts T_{MT} to higher values with little influence on T_C^A . Earlier studies showed that the Mn and total magnetic moments in Ni_2MnSn alloys diminish with the reduction in $d_{Mn}-d_{Mn}$ [63].

In the present study, it was demonstrated that with increasing In concentration in the $Ni_{48}Mn_{39.5}Sn_{12.5-x}In_x$ alloy, the T_{MT}

increased, whereas the T_C^A changed little. This occurred in opposition to the increasing e/a and the larger atomic radius of In, whose introduction was expected to expand the unit cell volume. Although the EDS analysis showed that e/a changed little in the case of the bulk samples, it nonetheless changed more consistently in the case of ribbon samples, decreasing with increasing amount of In, and despite this occurrence, the T_{MT} shifted towards higher temperatures. This clearly is in agreement with the theoretical predictions and points out to the hybridization phenomena and changes in the magnetic contribution to the free energy [5, 64]. On the whole, the magnetic moment was found to diminish with increasing In content, what suggested upset ferromagnetic exchange in both the austenite and martensite. From Fig. 3d, it is clear that the magnetization at 4 K dropped at the level of $0.05 \mu_B/Mn$ per 1 at.% of In, what is likely related to the changes in $d_{Mn}-d_{Mn}$ distance executed when In occupies Sn sites. This effect is further consistent with the results obtained when Co and Fe were substituted for Mn in the Ni–Mn–Sn alloy [18]. It was there shown that despite increasing e/a , the T_{MT} dropped and the effect was explained from theoretical calculations in terms of the increasing formation energy [18]. Thus, in the present scenario, the increase in T_{MT} can be justified by strengthening hybridization, which stabilizes the martensite phase against austenite. The increasing T_{MT} then coincides with the T_C^A leading effectively to a weak magnetic to paramagnetic reverse MT in the case of the In6 alloy ($T_C^A \ll A_s$), which produced the lowest $\Delta S_{transf.}^{mag.}$ and $\Delta T_{ad.}$. Interestingly, despite the lower than in the In2 magnetization, the largest entropy and temperature changes were observed for the In4 alloy. This was due to a large magnetization change on the order of 28 and 26 A/m²kg (Fig. 4) for bulk and ribbon alloys, respectively. The $\Delta T_{ad.}$ under 1.7 T gave 1.3 K, which can significantly increase under larger magnetic field with prospects for solid-state refrigeration.

Overall, it was demonstrated that the e/a and the chemical pressure rules of thumb are not the sole factors controlling the evolution of the T_{MT} and T_C^A in metamagnetic Ni–Mn–Sn alloys. It turns out that in agreement with the more theoretical predictions, hybridization phenomena and magnetic contribution into the Gibbs free energy change can exert a stronger influence on a stability of a given system often undermining the more experimentally established e/a rule.

Conclusions

The In for Sn substitution in the $Ni_{48}Mn_{39.5}Sn_{12.5-x}In_x$ bulk and ribbon alloys was studied. In contradiction to the established e/a and the chemical pressure rules, it was found that martensitic transformation temperature increases, while Sn is replaced with In. the magnetic entropy changes under 5 T applied magnetic field yielded 20.4 and 14.4 J/kgK in $Ni_{48}Mn_{39.5}Sn_{8.5}In_4$ bulk and ribbon alloy, respectively. The corresponding adiabatic

temperature change under 1.7 T produced 1.3 K temperature change for the same alloy. The observed behavior of characteristic transformation temperature and magnetization changes are consistent with theoretical predictions, and overall, they are interesting for the development of magnetocaloric Heusler-based alloys.

Methods

Polycrystalline alloys with nominal compositions of $\text{Ni}_{48}\text{Mn}_{39.5}\text{Sn}_{12.5-x}\text{In}_x$ ($x=2, 4, 6$) were manufactured from pure (>>99.9%) elements by conventional induction casting. Parts of master ingots were then melt spun on a rotating (50 Hz) copper drum. The ingots were sealed in quartz capsules and annealed at 1070 K and at 1170 K for 24 h to ensure chemical homogeneity. Homogenization was concluded with water quenching. The alloys are hereafter referred to as In2, In4, and In6 bulk and ribbons. The resulting chemical compositions of bulk alloys and ribbons were evaluated with a FEI-ESEM XL-30 scanning electron microscope (SEM) equipped with an EDX detector. The alloys were identified with the following average compositions for bulk: $\text{Ni}_{49.7}\text{Mn}_{38.1}\text{Sn}_{10}\text{In}_{2.1}$ ($e/a=8.11$), $\text{Ni}_{50.5}\text{Mn}_{37.5}\text{Sn}_{8.2}\text{In}_{3.8}$ ($e/a=8.12$), $\text{Ni}_{50.7}\text{Mn}_{37.5}\text{Sn}_{6.2}\text{In}_{5.6}$ ($e/a=8.11$); and ribbons: $\text{Ni}_{49.8}\text{Mn}_{37.8}\text{Sn}_{10.1}\text{In}_{2.2}$ ($e/a=8.10$), $\text{Ni}_{49.6}\text{Mn}_{37.7}\text{Sn}_{8.4}\text{In}_{4.3}$ ($e/a=8.06$), $\text{Ni}_{50.3}\text{Mn}_{37.4}\text{Sn}_{6.2}\text{In}_{6.1}$ ($e/a=8.08$). The crystal structures and phase purity were identified with X-ray diffraction (XRD) by means of an Empyrean PANalytical diffractometer. Diffracted beam graphite monochromator and an X'Celerator linear detector (Ag K_α radiation) were used. The XRD patterns were analyzed using the Full Proof software [65] based on the Rietveld method. The background intensity was refined with a polynomial, and the peak shape was approximated with a pseudo-Voigt function. The microstructure was studied using Tecnai G2 (200 kV) transmission electron microscope. Thin foils for TEM inspections were prepared by TenuPol-5 double jet electropolisher and an electrolyte of nitric acid (1/3 vol.) and methanol (2/3 vol.) cooled to 240 K. Thermal effects were studied with differential scanning calorimetry (DSC) with 10 K/min heating rate applied with Q1000 TA instrument. The DC magnetic susceptibility and magnetization were examined by Vibrating Sample Magnetometer (VSM) option of the Quantum Design Physical Property Measurement System (PPMS-9) in the temperature range from 2 to 380 K and in the magnetic field of 5 mT (and 5 T). In order to determine the actual temperature change the adiabatic temperature changes (ΔT_{ad}) for bulk alloys were measured under magnetic field from 0.5 to 1.7 T at temperatures close the T_{MT} using a homemade apparatus. Ribbons were omitted in this evaluation since they show lower $\Delta S_{\text{transf}}^{\text{mag}}$ than bulk alloys.

Acknowledgments

The financial support from the Ministry of Science and Higher Education of Poland under the scope of statutory works (Z-12) is gratefully acknowledged.

Data availability

Derived data supporting the findings of this study are provided with the paper or they are available from the corresponding author upon request.

Declarations

Conflict of interest On behalf of all authors, the corresponding author states that there is no conflict of interest.

Open Access

This article is licensed under a Creative Commons Attribution 4.0 International License, which permits use, sharing, adaptation, distribution and reproduction in any medium or format, as long as you give appropriate credit to the original author(s) and the source, provide a link to the Creative Commons licence, and indicate if changes were made. The images or other third party material in this article are included in the article's Creative Commons licence, unless indicated otherwise in a credit line to the material. If material is not included in the article's Creative Commons licence and your intended use is not permitted by statutory regulation or exceeds the permitted use, you will need to obtain permission directly from the copyright holder. To view a copy of this licence, visit <http://creativecommons.org/licenses/by/4.0/>.

References

1. X. Moya, L.L. Manosa, A. Planes, T. Krenke, M. Acet, E.F. Wassermann, Martensitic transition and magnetic properties in Ni-Mn-X alloys. *Mater. Sci. Eng. A* **438–440**, 911–915 (2006)
2. T. Krenke, X. Moya, S. Aksoy, M. Acet, P. Entel, L.L. Manosa, A. Planes, Y. Elerman, A. Yucel, E.F. Wassermann, Electronic aspects of the martensitic transition in Ni-Mn based Heusler alloys. *J. Magn. Magn. Mater.* **310**, 2788–2789 (2007)
3. M. Khan, I. Dubenko, S. Stadler, N. Ali, Magnetic and structural phase transitions in Heusler type alloys $\text{Ni}_2\text{MnGa}_{1-x}\text{In}_x$. *J. Phys. Condens. Matter* **16**, 5259–5266 (2004)
4. M. Ye, A. Kimura, Y. Miura, M. Shirai, Y.T. Cui, K. Shimada, H. Namatame, M. Taniguchi, S. Ueda, K. Kobayashi, R. Kainuma, T. Shishido, K. Fukushima, T. Kanomata, Role of electronic structure in the martensitic phase transition of $\text{Ni}_2\text{Mn}_{1+x}\text{Sn}_{1-x}$

- studied by hard X-ray photoelectron spectroscopy and ab initio calculations. *Phys. Rev. Lett.* **104**, 176401 (2010)
5. V. Sanchez-Alarcos, V. Recarte, J.I. Perez-Landazabal, C. Gomez-Polo, J.A. Rodriguez-Velamazan, Role of magnetism on the martensitic transformation in Ni-Mn-based magnetic shape memory alloys. *Acta Mater.* **60**, 459–468 (2012)
 6. T. Krenke, M. Acet, E.F. Wassermann, X. Moya, L.L. Manosa, A. Planes, Martensitic transitions and the nature of ferromagnetism in the austenitic and martensitic states of Ni-Mn-Sn alloys. *Phys. Rev. B* **72**, 014412 (2005)
 7. W. Maziarz, P. Czaja, M.J. Szczerba, L. Lityńska-Dobrzyńska, T. Czeppe, J. Dutkiewicz, Influence of Ni/Mn concentration ratio on microstructure and martensitic transformation in melt-spun Ni-Mn-Sn Heusler alloy ribbons. *J. Alloy. Compd.* **615**, S173–S177 (2014)
 8. T. Krenke, E. Duman, M. Acet, X. Moya, L.L. Manosa, A. Planes, Effect of Co and Fe on the inverse magnetocaloric properties of Ni-Mn-Sn. *J. Appl. Phys.* **102**, 033903 (2007)
 9. J. Chen, Z. Han, B. Qian, P. Zhang, D. Wang, Y. Du, The influence of Al substitution on the phase transitions and magnetocaloric effect in $\text{Ni}_{43}\text{Mn}_{46}\text{Sn}_{11-x}\text{Al}_x$ alloys. *J. Magn. Magn. Mater.* **323**, 248–251 (2011). <https://doi.org/10.1016/j.jmmm.2010.09.015>
 10. W. Maziarz, P. Czaja, M.J. Szczerba, J. Przewoźnik, C. Kapusta, A. Żywczak, T. Stobiecki, E. Cesari, J. Dutkiewicz, Room temperature magnetostructural transition in Al for Sn substituted Ni-Mn-Sn melt spun ribbons. *J. Magn. Magn. Mater.* **348**, 8–16 (2013)
 11. S. Chatterjee, S. Giri, S.K. De, S. Majumdar, Giant magnetocaloric effect near room temperature in Ni-Mn-Sn-Ga alloys. *J. Alloys Compd.* **503**, 273–276 (2010)
 12. Z.D. Han, D.H. Wang, C.L. Zhang, H.C. Xuan, J.R. Zhang, B.X. Gu, Y.W. Du, Effect of lattice contraction on martensitic transformation and magnetocaloric effect in Ge doped Ni-Mn-Sn alloys. *Mater. Sci. Eng. B* **157**, 40–43 (2009)
 13. H.C. Xuan, P.D. Han, D.H. Wang, Y.W. Du, The influence of Ge substitution on the magnetostucture transition and magnetocaloric effect of Mn–Ni–Sn–Ge alloys. *J. Alloys Compd.* **582**, 369–373 (2014). <https://doi.org/10.1016/j.jallcom.2013.08.053>
 14. P. Czaja, J. Przewoźnik, C. Kapusta, W. Maziarz, The Ge enhanced exchange bias effect in $\text{Ni}_{50}\text{Mn}_{37.5}\text{Sn}_{12.5}$ metamagnetic shape memory alloys. *Mater. Res. Express* **6**, 106111 (2019)
 15. W. Maziarz, P. Czaja, A. Wójcik, J. Dutkiewicz, J. Przewoźnik, E. Cesari, Microstructure and martensitic transformation of $\text{Ni}_{50}\text{Mn}_{37.5}\text{Sn}_{12.5-x}\text{Gex}$ ($x = 0, 1, 2, 3$) Heusler alloys produced by various technologies. *Mater. Today* **2S**, S523–S528 (2015)
 16. H.C. Xuan, D.H. Wang, C.L. Zhang, Z.D. Han, H.S. Liu, B.X. Gu, Y.W. Du, The large low-field magnetic entropy changes in $\text{Ni}_{43}\text{Mn}_{46}\text{Sn}_{11-x}\text{Sb}_x$ alloys. *Solid State Commun.* **142**, 591–594 (2007)
 17. M. Khan, J. Jung, S.S. Stoyko, A. Mar, A. Quetz, T. Samanta, I. Dubenko, N. Ali, S. Stadler, K.H. Chow, The role of Ni-Mn hybridization on the martensitic phase transitions in Mn-rich Heusler alloys. *Appl. Phys. Lett.* **100**, 172403 (2012)
 18. X. Wang, J.X. Shang, F.H. Wang, C.B. Jiang, H.B. Xu, Origin of unusual properties in the ferromagnetic Heusler alloy Ni-Mn-Sn: a first-principles investigation. *Scripta Mater.* **89**, 33–36 (2014)
 19. H.B. Xiao, C.P. Yang, R.L. Wang, V.V. Marchenkov, X. Luo, Martensitic transformation and phase stability of In-doped Ni-Mn-Sn shape memory alloys from first-principles calculations. *J. Appl. Phys.* **115**, 203703 (2014)
 20. W. Maziarz, A. Wójcik, P. Czaja, A. Żywczak, J. Dutkiewicz, Ł. Hawełek, E. Cesari, Magneto-structural transformations in $\text{Ni}_{50}\text{Mn}_{37.5}\text{Sn}_{12.5-x}\text{In}_x$ Heusler powders. *J. Magn. Magn. Mater.* **412**, 123–131 (2016)
 21. Z. Guo, L. Pan, M. Yasir-Rafique, X. Zheng, H. Qiu, Z. Liu, Metamagnetic phase transformation and magnetocaloric effect in quinary $\text{Ni}_{45}\text{Co}_5\text{Mn}_{40}\text{In}_x\text{Sn}_{10-x}$ Heusler alloy. *J. Alloys Compd.* **577**, 174–178 (2013)
 22. S. Dwevedi, B. Tiwari, Martensitic transformations and magnetocaloric effect in Sn-doped NiMnIn shape memory alloy. *J. Alloys Compd.* **540**, 16–20 (2012)
 23. W. Maziarz, P. Czaja, J. Dutkiewicz, R. Wróblewski, M. Leonowicz, Magnetic and martensitic transformations in $\text{Ni}_{46}\text{Mn}_{41.5-x}\text{Fe}_x\text{Sn}_{12.5}$ melt spun ribbons. *Mater. Sci. Forum* **782**, 23–30 (2014)
 24. Y. Wang, Ch. Huang, J. Gao, S. Yang, X. Ding, X. Song, X. Ren, Evidence for ferromagnetic strain glass in Ni-Co-Mn-Ga Heusler alloy system. *Appl. Phys. Lett.* **101**, 101913 (2012). <https://doi.org/10.1063/1.4751250>
 25. P. Czaja, A. Wierzbicka-Miernik, Ł. Rogal, Segregation and microstructure evolution in chill cast and directionally solidified Ni-Mn-Sn metamagnetic shape memory alloys. *J. Cryst. Growth.* **492**, 50–59 (2018)
 26. W.M. Yuhasz, D.L. Schlager, Q. Xing, K.W. Dennis, R.W. McCallum, T.A. Lograsso, Influence of annealing and phase decomposition on the magnetostructural transitions in $\text{Ni}_{50}\text{Mn}_{39}\text{Sn}_{11}$. *J. Appl. Phys.* **105**, 07A921 (2009)
 27. C. Segui, E. Cesari, Composition and atomic order effects on the structural and magnetic transformations in ferromagnetic Ni-Co-Mn-Ga shape memory alloys. *J. Appl. Phys.* **111**, 043914 (2012)
 28. P. Czaja, M. Kowalczyk, W. Maziarz, On the magnetic contribution to the inverse magnetocaloric effect in Ni-Co-Cu-Mn-Sn metamagnetic shape memory alloys. *J. Magn. Magn. Mater.* **474**, 381–392 (2019)
 29. M. Nazmunnahar, L. Gonzalez, J.J. del Val, J. Gonzalez, J.J. Sunol, B. Hernando, Martensitic transformation in $\text{Ni}_{50}\text{Mn}_{50-x}\text{Sn}_x$ ($x = 11, 125$) and $\text{Ni}_{49}\text{Mn}_{51-x}\text{Sn}_x$ ($x = 13$) Heusler alloy. *IEEE Trans. Magn.* **48**, 3749–3752 (2012)
 30. A. Planes, L.L. Manosa, X. Moya, T. Krenke, M. Acet, E.F. Wassermann, Magnetocaloric effect in Heusler shape-memory alloys. *J. Magn. Magn. Mater.* **310**, 2767–2769 (2007)

31. H. Zheng, W. Wang, S. Xue, Q. Zhai, J. Frenzel, Z. Luo, Composition-dependent crystal structure and martensitic transformation in Heusler Ni-Mn-Sn alloys. *Acta Mater.* **61**, 4648–4656 (2013)
32. K. Koyama, K. Watanabe, T. Kanomata, R. Kainuma, K. Oikawa, K. Ishida, Observation of field induced reverse transformation in ferromagnetic shape memory alloy $\text{Ni}_{50}\text{Mn}_{36}\text{Sn}_{14}$. *Appl. Phys. Lett.* **88**, 132505–132513 (2006)
33. Q. Tao, Z.D. Han, J.J. Wang, B. Qian, P. Zhang, X.F. Jiang, D.H. Wang, Y.W. Du, Phase stability and magnetic-field-induced martensitic transformation in Mn-rich NiMnSn alloys. *AIP Adv.* **2**, 042181–042188 (2012)
34. R. Kainuma, Y. Imano, W. Ito, Y. Sutou, H. Morito, S. Okamoto, O. Kitakami, K. Oikawa, A. Fujita, T. Kanomata, K. Ishida, Magnetic-field-induced shape recovery by reverse phase transformation. *Nature* **439**, 957–960 (2006). <https://doi.org/10.1038/nature04493>
35. Z.D. Han, D.H. Wang, C.L. Zhang, H.C. Xuan, B.X. Gu, Y.W. Du, Low-field inverse magnetocaloric effect in $\text{Ni}_{50-x}\text{Mn}_{39+x}\text{Sn}_{11}$ Heusler alloys. *Appl. Phys. Lett.* **90**, 042507–042513 (2007). <https://doi.org/10.1063/1.2435593>
36. E.C. Passamani, E. Lozano, C. Larica, C.A.C. Marcelo, W.L. Scopel, I. Merino, A.L. Alves, A.Y. Takeuchi, V.P. Nascimento, Influence of chemical pressure in Sn-substituted Ni_2MnGa Heusler alloy: experimental and theoretical studies. *J. Appl. Phys.* **112**, 073921–073926 (2012)
37. S. Esakki Muthu, N.V. Rama Rao, M. Manivel Raja, S. Arumugam, K. Matsubayasi, Y. Uwatoko, Hydrostatic pressure effect on the martensitic transition, magnetic, and magnetocaloric properties in $\text{Ni}_{50-x}\text{Mn}_{37+x}\text{Sn}_{13}$ Heusler alloys. *J. Appl. Phys.* **110**, 083902 (2011). <https://doi.org/10.1063/1.3651375>
38. E.C. Passamani, F. Xavier, E. Favre-Nicolin, C. Larica, A.Y. Takeuchi, I.L. Castro, J.R. Proveti, Magnetic properties of NiMn-based Heusler alloys influenced by Fe atoms replacing Mn. *J. Appl. Phys.* **105**, 033919–033928 (2009)
39. H.C. Xuan, Y.X. Zheng, S.C. Ma, Q.Q. Cao, D.H. Wang, Y.W. Du, The martensitic transformation, magnetocaloric effect, and magnetoresistance in high-Mn content $\text{Mn}_{47+x}\text{Ni}_{43-x}\text{Sn}_{10}$ ferromagnetic shape memory alloys. *J. Appl. Phys.* **108**, 103920 (2010)
40. F.S. Liu, Q.B. Wang, S.P. Li, W.Q. Ao, J.Q. Li, The martensitic transition and magnetocaloric properties of $\text{Ni}_{51}\text{Mn}_{49-x}\text{Sn}_x$. *Phys. B* **412**, 74–78 (2013)
41. R. Coll, L. Escoda, J. Saurina, J.L. Sanchez-Llamazares, B. Hernando, J.J. Sunol, Martensitic transformation in Mn–Ni–Sn Heusler alloys. *J. Therm. Anal. Calorim.* **99**, 905–909 (2010). <https://doi.org/10.1007/s10973-009-0489-2>
42. H.S. Liu, C.L. Zhang, Z.D. Han, H.C. Xuan, D.H. Wang, Y.W. Du, The effect of Co doping on the magnetic entropy changes in $\text{Ni}_{44-x}\text{Co}_x\text{Mn}_{45}\text{Sn}_{11}$ alloys. *J. Alloys Compd.* **467**, 27–30 (2009). <https://doi.org/10.1016/j.jallcom.2007.11.137>
43. D.Y. Cong, S. Roth, M. Potschke, C. Hurrich, L. Schultz, Phase diagram and composition optimization for magnetic shape memory effect in Ni–Co–Mn–Sn alloys. *Appl. Phys. Lett.* **97**, 021908 (2010). <https://doi.org/10.1063/1.3454239>
44. W. Ito, X. Xu, R.Y. Umetsu, T. Kanomata, K. Ishida, R. Kainuma, Concentration dependence of magnetic moment in $\text{Ni}_{50-x}\text{Co}_x\text{Mn}_{50-y}\text{Z}_y$ ($Z = \text{In, Sn}$) Heusler alloys. *Appl. Phys. Lett.* **97**, 242515 (2010)
45. I. Dincer, E. Yuzuak, Y. Elerman, Influence of irreversibility on inverse magnetocaloric and magnetoresistance properties of the $(\text{Ni, Cu})_{50}\text{Mn}_{36}\text{Sn}_{14}$ alloys. *J. Alloys Compd.* **506**, 508–512 (2010). <https://doi.org/10.1016/j.jallcom.2010.07.066>
46. C. Jing, Y.J. Yang, Z. Li, X.L. Wang, B.J. Kang, S.X. Cao, J.C. Zhang, J. Zhu, B. Lu, Tuning martensitic transformation and large magnetoresistance in $\text{Ni}_{50-x}\text{Cu}_x\text{Mn}_{38}\text{Sn}_{12}$ Heusler alloys. *J. Appl. Phys.* **113**, 173902 (2013)
47. R. Das, S. Sarma, A. Perumal, A. Srinivasan, Effect of Co and Cu substitution on the magnetic entropy change in $\text{Ni}_{46}\text{Mn}_{43}\text{Sn}_{11}$ alloy. *J. Appl. Phys.* **109**, 07A901 (2011). <https://doi.org/10.1063/1.3540327>
48. B. Gao, F.X. Hu, J. Shen, J. Wang, J.R. Sun, B.G. Shen, Field-induced structural transition and the related magnetic entropy change in $\text{Ni}_{43}\text{Mn}_{43}\text{Co}_3\text{Sn}_{11}$ alloy. *J. Magn. Magn. Mater.* **321**, 2571–2574 (2009). <https://doi.org/10.1016/j.jmmm.2009.03.047>
49. C.L. Zhang, W.Q. Zou, H.C. Xuan, Z.D. Han, D.H. Wang, B.X. Gu, Y.W. Du, Giant low-field magnetic entropy changes in $\text{Ni}_{45}\text{Mn}_{44-x}\text{Cr}_x\text{Sn}_{11}$ ferromagnetic shape memory alloys. *J. Phys. D: Appl. Phys.* **40**, 7287–7290 (2007). <https://doi.org/10.1088/0022-3727/40/23/005>
50. D.H. Wang, C.L. Zhang, Z.D. Han, H.C. Xuan, B.X. Gu, Y.W. Du, Large magnetic entropy changes and magnetoresistance in $\text{Ni}_{45}\text{Mn}_{42}\text{Cr}_2\text{Sn}_{11}$ alloy. *J. Appl. Phys.* **103**, 033901 (2008). <https://doi.org/10.1063/1.2836940>
51. F. Chen, Ch. Gong, Y. Guo, M. Zhang, Y. Chai, The effect of substitution of Ti for Mn on the martensitic transformation and magnetic entropy changes in Mn-rich $\text{Mn}_{48-x}\text{Ti}_x\text{Ni}_{42}\text{Sn}_{10}$ alloys. *Phys. Status Solidi A* **210**, 2762–2766 (2013). <https://doi.org/10.1002/pssa.201330154>
52. S. Li, Z. Lin, Z. Wang, J. Xu, L. Wang, J. Lin, Y. Hu, F. Xu, T.X. Nan, N.X. Sun, J.G. Duh, Large field-induced magnetocaloric effect in $\text{Ni}_{43}\text{Mn}_{46-x}\text{V}_x\text{Sn}_{11}$ Heusler alloys. *IEEE Trans. Magn.* **48**, 3985–3988 (2012). <https://doi.org/10.1109/TMAG.2012.2199284>
53. H.C. Xuan, D.H. Wang, C.L. Zhang, Z.D. Han, B.X. Gu, Y.W. Du, Boron's effect on martensitic transformation and magnetocaloric effect in $\text{Ni}_{43}\text{Mn}_{46}\text{Sn}_{11}\text{B}_x$ alloys. *Appl. Phys. Lett.* **92**, 102503 (2008). <https://doi.org/10.1063/1.2895645>
54. B. Gao, F. Shen, F.X. Hu, J. Wang, J.R. Sun, B.G. Shen, Magnetic properties and magnetic entropy change in Heusler alloys $\text{Ni}_{50}\text{Mn}_{35-x}\text{Cu}_x\text{Sn}_{15}$. *Appl. Phys. A* **97**, 443–447 (2009). <https://doi.org/10.1007/s00339-009-5239-6>
55. D.H. Wang, C.L. Zhang, H.C. Xuan, Z.D. Han, J.R. Wang, J.R. Zhang, S.L. Tang, B.X. Gu, Y.W. Du, The study of low-field positive and negative magnetic entropy changes in

- $\text{Ni}_{43}\text{Mn}_{46-x}\text{Cu}_x\text{Sn}_{11}$ alloys. *J. Appl. Phys. Lett.* **102**, 013909 (2007). <https://doi.org/10.1063/1.2752140>
56. Z. Liu, Z. Wu, H. Yang, Y. Liu, W. Wang, X. Ma, G. Wu, Martensitic transformation and magnetic properties in ferromagnetic shape memory alloy $\text{Ni}_{43}\text{Mn}_{46}\text{Sn}_{11-x}\text{Si}_x$. *Intermetallics* **19**, 1605–1611 (2011). <https://doi.org/10.1016/j.intermet.2011.06.007>
 57. R. Saha, A.K. Nigam, Room temperature inverse magnetocaloric effect in Pd substituted $\text{Ni}_{50}\text{Mn}_{37}\text{Sn}_{13}$ Heusler alloys. *Phys. B* **448**, 263–266 (2014). <https://doi.org/10.1016/j.physb.2014.04.011>
 58. P. Czaja, W. Maziarz, J. Przewoźnik, C. Kapusta, L. Hawelek, A. Chrobak, P. Drzymała, M. Fitta, A. Kolano-Burian, Magnetocaloric properties and exchange bias effect in Al For Sn substituted $\text{Ni}_{48}\text{Mn}_{39.5}\text{Sn}_{12.5}$ Heusler alloy ribbons. *J. Magn. Magn. Mater.* **358–359**, 142–148 (2014)
 59. S. Agarwal, P.K. Mukhopadhyay, The effect of Al replacement and heat treatment on magnetocaloric properties of $\text{Ni}_2\text{Mn-Sn}$ ferromagnetic shape memory alloys. *J. Alloys Compd.* **608**, 329–333 (2014)
 60. H.B. Xiao, C.P. Yang, R.L. Wang, V.V. Marchenkov, K. Barner, *J. Appl. Phys.* **112**, 123723–123725 (2012)
 61. Y. Chieda, T. Kanomata, K. Fukushima, K. Matsubayashi, Y. Uwatoko, R. Kainuma, K. Oikawa, K. Ishida, K. Obara, T. Shishido, Magnetic properties of Mn-rich Ni_2MnSn Heusler alloys under pressure. *J. Alloys Compd.* **486**, 51–54 (2009). <https://doi.org/10.1016/j.jallcom.2009.06.206>
 62. S. Esakki Muthu, N.V. Rama Rao, M. Manivel Raja, S. Arumugam, K. Matsubayasi, Y. Uwatoko, Hydrostatic pressure effect on the martensitic transition, magnetic, and magnetocaloric properties in $\text{Ni}_{50-x}\text{Mn}_{37+x}\text{Sn}_{13}$ Heusler alloys. *J. Appl. Phys.* **110**, 083902 (2011)
 63. E. Sasioglu, L.M. Sandratskii, P. Bruno, First-principles calculation of the intersublattice exchange interactions and Curie temperatures of the full Heusler alloys Ni_2MnX ($X = \text{Ga, In, Sn, Sb}$). *Phys. Rev. B* **70**, 024427 (2004)
 64. R.H. Kou, J. Gao, Y. Ren, B. Sanyal, S. Bhandary, S.M. Heals, B. Fisher, C.J. Sun, Charge transfer-tuned magnetism in Nd-substituted Gd_5Si_4 . *AIP Adv.* **8**, 125219 (2018). <https://doi.org/10.1063/1.5081457>
 65. J. Rodriguez-Carvajal, Recent advances in magnetic structure determination by neutron powder diffraction. *Phys. B* **192**(1–2), 55–69 (1993). [https://doi.org/10.1016/0921-4526\(93\)90108-I](https://doi.org/10.1016/0921-4526(93)90108-I)